Theoretical treatment of pseudorotation in the Jahn-Teller C_{60}^{+} ion

Ian D. Hands, Lubna M. Sindi, Janette L. Dunn,* and Colin A. Bates
School of Physics and Astronomy, University of Nottingham, Nottingham, NG7 2RD, United Kingdom
(Received 25 May 2006; published 22 September 2006)

A theoretical investigation of the pseudorotational dynamics in the C_{60}^{+} cation is made using a single-mode $H\otimes h$ model. Analytical expressions for the rate of pseudorotation are formulated as a function of the vibronic coupling parameters and used to probe the dynamics of the Jahn-Teller effect. For particular values of the coupling constants, it is known that the ground state of the system may change from the expected H symmetry to one of A symmetry. Therefore, we examine the dynamics in the coupling regime where this ground-state H-A crossover occurs. Using coupling constants taken from the literature, a pseudorotational period of ~210 fs is estimated for this ion. Thus there is the potential that pseudorotation could be observed in ultrafast optical experiments.

DOI: 10.1103/PhysRevB.74.115410 PACS number(s): 61.48.+c, 31.30.Gs, 71.70.Ej

I. INTRODUCTION

Electron-doped derivatives of the fullerene C_{60} have attracted considerable attention over recent years. Much of this is because of their potential to exhibit high-temperature superconductivity.[1–4] More recently, attention has been widened to include the hole-doped derivatives of C_{60} as these are expected to have critical temperatures that exceed their negatively doped counterparts.[5] The mechanism for superconductivity in these fullerene derivatives is not completely understood, but it does seem likely that the intramolecular Jahn-Teller (JT) effect plays an important part in the process.[4,6] Therefore, investigation of the nature of the JT effect in these ions is paramount.

According to Hückel molecular orbital theory, C_{60} has a highest occupied molecular orbital of H_u symmetry.[7] Group theory indicates that the C_{60}^{+} ion will be subject to a $H_u\otimes(6g_g+8h_g)$ JT effect, wherein six g_g and eight h_g normal modes of vibration are coupled to the H_u electronic ground state of the ion.[8] However, density functional calculations[5,9] indicate that in C_{60}^{+} the coupling to the h_g modes is much stronger than it is to modes of g_g symmetry. Therefore, we can begin our investigations of vibronic coupling in the C_{60}^{+} cation by considering a $H\otimes h$ JT model.

The JT coupling instantaneously distorts a C_{60}^{+} ion into one of several isoenergetic configurations of reduced symmetry, each of which differs in its relative orientation in space. Over a period of time, the ion can interconvert between these different configurations to produce a system whose symmetry is, on average, icosahedral. Such interconversions are generally described as pseudorotations because, unlike real molecular rotation, no angular momentum is associated with the process. Evidence for this JT effect in C_{60}^{+} may be found in the photoemission spectrum (PES) of gaseous C_{60},[10] where the occurrence of three tunneling states in the data was interpreted in terms of distortion of the C_{60}^{+} ions into species of D_{3d} symmetry. However, this interpretation has been questioned by other workers,[11] who do not agree that the PES data necessarily point to cations that are of D_{3d} symmetry.

Ultrafast pump-probe spectroscopy has already been successfully used to investigate the rate at which pseudorotation occurs in the simple Na_3 cluster[12] (an $E\otimes e$ JT system). Thus, we may expect that the rate of pseudorotation in more complicated systems, such a those presented by the $C_{60}^{n\pm}$ ions, may be discernible in the near future. The rate at which pseudorotation occurs must, of course, depend on the shape of the lowest adiabatic potential energy surface (APES), which, in turn, will depend on the vibronic coupling parameters. Hence, determination of pseudorotation rates must give information about the strength and nature of the underlying vibronic coupling.

In this work, we make a simple application of the time evolution operator to derive analytic expressions for the rates of pseudorotation for the general $H\otimes h$ JT system. The theory is developed for instances in which only the lowest vibronic levels play any significant role and is therefore most appropriate to studies at low absolute temperature or where the lowest vibronic levels are selected spectroscopically. In this system, there are two possible types of linear vibronic coupling, which lead to minima in the APES of either pentagonal (D_{5d}) or trigonal (D_{3d}) symmetry.[8,13] Pseudorotation rates are derived for both cases. The case of trigonal minima has a particularly interesting facet in that it is possible, for sufficiently strong vibronic coupling, for the system to form a ground state of A rather than the expected H symmetry.[14,15] Using the theory, we investigate the pseudorotation dynamics in the regime where this H-A crossover occurs.

Finally, application to the C_{60}^{+} ion is made using calculated coupling constants taken from the literature in order to estimate the pseudorotation rate appropriate for this ion. A discussion will be given of the expected effects of including coupling to all g_g and h_g modes.

II. THEORY

A general theory that may be used to follow the temporal evolution of a dynamically distorted JT system has been given in an earlier publication,[16] where the theory was used to investigate pseudorotation in $E\otimes e$ systems. The theory has also been extended to the $T\otimes h$ system applicable to C_{60}^{-} anions.[17] Therefore, for the sake of brevity, only a concise outline of the method used will be given here.

For the $H\otimes h$ JT coupling problem, the Hamiltonian for the system takes the form

$$\mathcal{H} = \mathcal{H}_0 + \mathcal{H}_1(\mathbf{Q}) + \mathcal{H}_2(\mathbf{Q}), \tag{1}$$

where $\mathcal{H}_0 = \frac{1}{2}\Sigma_i(P_i^2/\mu + \mu\omega^2 Q_i^2)$ is the Hamiltonian for the uncoupled oscillator system of mass μ, and $\mathcal{H}_1$ and $\mathcal{H}_2$ are the two types of linear interaction Hamiltonian which depend explicitly and linearly on the h-type phonon mode $\mathbf{Q} = (Q_\theta, Q_\varepsilon, Q_4, Q_5, Q_6)$. The two types of linear coupling arise as the Kronecker square $H\otimes H$ contains the H irreducible representation twice.[8]

The JT interaction distorts the ion away from icosahedral symmetry so that it acquires either D_{3d} or D_{5d} geometry, depending on the relative contributions of $\mathcal{H}_1$ and $\mathcal{H}_2$ in Eq. (1). [8] The notation used here is that of Ref. 14—namely, that $\mathcal{H}_1$ represents the interaction that produces D_{3d} (also referred to as trigonal) wells, whereas $\mathcal{H}_2$ generates wells with D_{5d} (pentagonal) symmetry. We will define dimensionless linear vibronic coupling constants associated with $\mathcal{H}_1$ and $\mathcal{H}_2$ to be V_1'' and V_1', respectively. Thus the D_{5d} wells depend upon the coupling constant V_1' only and the D_{3d} wells on V_1'' only. We note in passing that distortion into D_{2h} and C_{2h} geometries is not favored in this system, although such minima are possible in the multiply doped cations such as C_{60}^{2+}.[18,19]

In the limit of infinitely strong JT coupling, the $H\otimes h$ system becomes locked into either one of six isoenergetic D_{5d} wells or one of ten isoenergetic D_{3d} wells. The wells will be denoted as $|w_i\rangle$. None of these wells have the symmetry required in order to be an eigenstate of the original Hamiltonian given in Eq. (1). However, we can use projection operators to generate combinations of the wells that do have the required symmetry. Thus, we denote by $|\Gamma_i\rangle$ the ith symmetry-adapted state (SAS) derived. Alternatively, we can express the states associated with the wells in terms of these SAS's,

$$|w_i\rangle = \sum_{j=1}^{n} b_i^{(j)} |\Gamma_j\rangle, \tag{2}$$

where the $b_i^{(j)}$ are real coefficients. The SAS's are good approximations to the true eigenstates of the system, and so we forthwith assume that we may use $\mathcal{H}|\Gamma_i\rangle = \mathcal{E}_i|\Gamma_i\rangle$ where $\mathcal{E}_i$ is the energy of the ith SAS. This assumption makes it simple to follow the temporal evolution of the system using the time evolution operator $U_t(t) = \exp(-i\mathcal{H}t/\hbar)$.

The probability P_{if} that a system starts off localized in an initial well $|w_i\rangle$ and becomes localized in another well $|w_f\rangle$ a time t later is found to be[16]

$$P_{if} = |\langle w_f|U_t|w_i\rangle|^2 = P_{if}^{(0)} - 4\sum_{j<k} b_i^{(j)} b_i^{(k)} b_f^{(j)} b_f^{(k)} \sin^2[(\mathcal{E}_j - \mathcal{E}_k)t/2\hbar], \tag{3}$$

where $P_{if}^{(0)}$ is the initial probability given by

$$P_{if}^{(0)} = \sum_j (b_i^{(j)} b_f^{(j)})^2 + 2\sum_{j<k} b_i^{(j)} b_i^{(k)} b_f^{(j)} b_f^{(k)}. \tag{4}$$

We can use Eqs. (3) and (4) to follow the temporal development of a system initially localized in a particular well. As can be seen from Eq. (3), the temporal characteristics depend on the energy differences $(\mathcal{E}_j - \mathcal{E}_k)$ between the various SAS's.

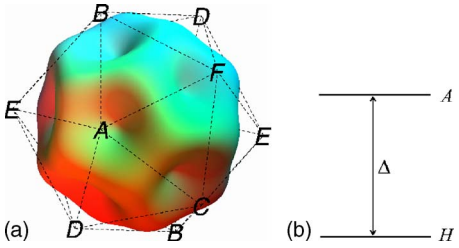

FIG. 1. (Color online) (a) A pictorial representation of the pentagonal wells and (b) the energies of the corresponding symmetry-adapted states formed from the well states. The well labels in (a) correspond to those defined in Ref. 20.

III. RESULTS

In order to model a real C_{60}^+ ion, consideration must be given to simultaneous coupling to all eight h_g modes of vibration (and possibly the six g_g modes). However, the overall result in this multimode problem is an ion exclusively possessing D_{5d} or D_{3d} wells. As these arise from either $\mathcal{H}_1$ or $\mathcal{H}_2$, we shall consider separately the problems with either $\mathcal{H}_1 \equiv 0$ or $\mathcal{H}_2 \equiv 0$. It should be mentioned that the calculated coupling constants for C_{60}^+ suggest that it is the $h_g(1)$ mode ($\sim$261 cm^{-1}) that is, by far, the most strongly coupled mode.[5] We would therefore expect the case where $\mathcal{H}_1 = 0$ (with D_{5d} minima) to be a very good approximation to the real C_{60}^+ ion. However, the actual coupling strengths pertinent to C_{60}^+ are yet to be determined quantitatively via experiment. It is also possible that other perturbations may favor the formation of D_{3d} minima. In addition, other JT systems subject to a $H\otimes h$ JT effect may be found in the future which form D_{3d} minima. For this reason and for the intrinsic interest in the results due to the presence of the H-A ground-state crossover, the pseudorotational behavior in the presence of these minima will also be considered.

A. Pentagonal minima

The definition of $\mathcal{H}_2$, which leads to the formation of pentagonal wells, and the ensuing expressions for the symmetry-adapted states have been given previously.[20] A representation of the wells and the relative energies of the symmetry-adapted states are shown schematically in Fig. 1. The tunneling splitting in this case has the explicit form

$$\Delta = -\frac{6S_p \ln S_p}{(1-S_p)(5+S_p)}\hbar\omega, \tag{5}$$

where

$$S_p = \exp\left[-\tfrac{12}{25}(V_1')^2\right] \tag{6}$$

is the phonon overlap between any two pentagonal wells (which are all equally separated). The variation of the tunneling splitting as a function of V_1' is shown in Fig. 2.

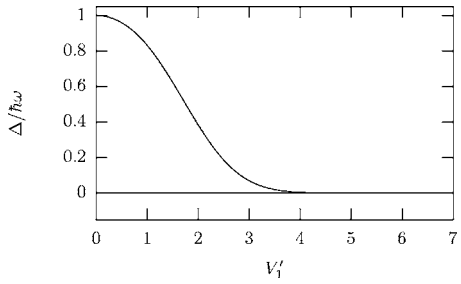

FIG. 2. A plot of the tunneling splitting Δ between the A and H symmetry-adapted states as a function of the dimensionless linear coupling constant V_1'.

Using the expressions for the (normalized) SAS's from Ref. 20, we can derive expressions for (normalized) states associated with the pentagonal wells. For example, for wells A and B (Fig. 1),

$$|A\rangle = \frac{|A_a^{(p)}\rangle}{\sqrt{6}N_A^{(p)}} + \frac{\sqrt{3}|H_\theta^{(p)}\rangle + |H_\varepsilon^{(p)}\rangle + \sqrt{6}|H_4^{(p)}\rangle}{2\sqrt{3}N_H^{(p)}},$$

$$|B\rangle = \frac{|A_a^{(p)}\rangle}{\sqrt{6}N_A^{(p)}} + \frac{\sqrt{3}|H_\theta^{(p)}\rangle + |H_\varepsilon^{(p)}\rangle - \sqrt{6}|H_4^{(p)}\rangle}{2\sqrt{3}N_H^{(p)}}, \tag{7}$$

where $|A_a^{(p)}\rangle$ is the SAS of A symmetry built from the pentagonal well states and $|H_j^{(p)}\rangle$ $(j=\theta,\epsilon,4,5,6)$ are the components of the corresponding SAS of H symmetry. In these expressions, each well state is normalized and $N_A^{(p)}$ and $N_H^{(p)}$ are normalization factors appearing in the expressions for the SAS's, given by

$$N_A^{(p)} = (1-S_p)^{-1/2},$$

$$N_H^{(p)} = \sqrt{5}(5+S_p)^{-1/2}. \tag{8}$$

It is now a simple matter to use Eq. (3) to derive the probabilities of finding the system in a particular well at time t:

$$P_{AA}(t) = 1 - \tfrac{1}{9}(1-S_p)(5+S_p)\sin^2(\Delta t/2\hbar),$$

$$P_{AB}(t) = \tfrac{1}{25}[5+S_p^2-5P_{AA}(t)], \tag{9}$$

where $P_{AX}(t)$ is the probability that a system initially localized in well A has migrated to well X at time t. Plots of these functions for the case of moderately strong vibronic coupling are shown in Fig. 3.

An interesting observation here is that $P_{AA} \geq 4/9$ at all times and for all coupling strengths. That is, if we initially localize the state in well A, then the probability of finding the system in well A subsequently never drops below 4/9. This behavior should be contrasted with that obtained for pseudorotation between pentagonal wells in the C_{60}^- ion,[17] where the minimum in P_{AA} is equal to the square of the phonon overlap between wells, which is very small in strong coupling. Therefore the pentagonal wells in the C_{60}^- ion seem to be much more discrete than in the present case.

Interpretation of the probabilities shown in Fig. 3 is straightforward. At $t=0$, the system migrates from well A and starts to appear in one of the adjacent wells. After a time

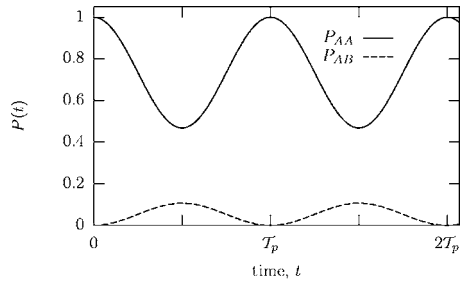

FIG. 3. Interwell dynamics for a pentagonal system initially localized in well A. $\mathcal{T}_p = 2\pi\hbar/\Delta$ is a characteristic pseudorotational time—i.e., the time taken for the initial localization to be regained. The plots correspond to moderately strong coupling $V_1'=2.50$ ($S_p=0.05$).

$t=\pi\hbar/\Delta$, the probability that well B, say, has become occupied reaches a maximum and the system begins to migrate back to well A. When $t=2\pi\hbar/\Delta$, the system has returned to its initial state, so that a complete pseudorotational circuit has occurred. Thus, we will define the pseudorotational period in this case as

$$\mathcal{T}_p = \frac{2\pi\hbar}{\Delta}, \tag{10}$$

where the subscript p is used to denote pseudorotation between pentagonal wells.

B. Trigonal minima

The definition of $\mathcal{H}_1$ used here is that given in Ref. 14, which also gives expressions for the symmetry-adapted states and their energies obtained using the procedure outlined in Sec. II. A representation of the trigonal wells and the energies of the symmetry-adapted states thus obtained is shown schematically in Fig. 4.

For completeness, we give here expressions for the tunneling splittings Δ_1 and Δ_2 shown in Fig. 4:

$$\Delta_1 = \frac{2(1-8S_t-2S_t^2)S_t \ln S_t}{(1-S_t)(1+2S_t)(3+S_t+2S_t^2)}\hbar\omega,$$

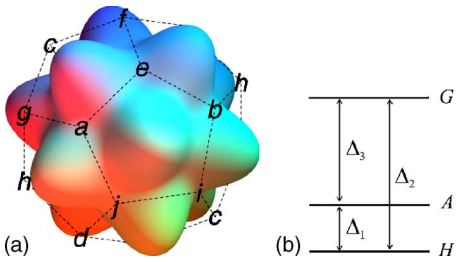

FIG. 4. (Color online) (a) A pictorial representation of the trigonal wells. The well labels correspond to those defined in Ref. 14. (b) The relative energies of the corresponding symmetry-adapted states formed by combining the trigonal wells to give states of the correct symmetry.

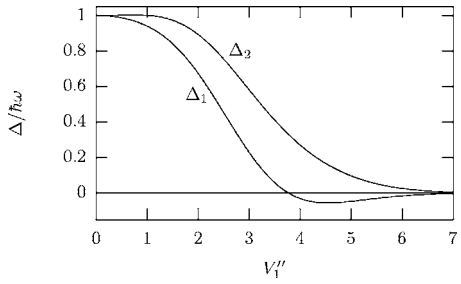

FIG. 5. Tunneling splittings between the A (Δ_1) and G (Δ_2) symmetry-adapted states and the H state (zero energy) as a function of the dimensionless linear coupling constant V_1'.

$$\Delta_2 = -\frac{3(3+6S_t-S_t^2)S_t \ln S_t}{(1-S_t)(3+S_t)(3+S_t+2S_t^2)}\hbar\omega, \tag{11}$$

where

$$S_t = \exp\left[-\tfrac{4}{27}(V_1'')^2\right] \tag{12}$$

is the phonon overlap between adjacent trigonal wells. In this form, it is easy to identify the phonon overlap S_t^X at the H-A crossover ($\Delta_1=0$) as[14]

$$S_t^X = 3/\sqrt{2} - 2 \approx 0.121, \tag{13}$$

corresponding to $V_1'' \approx 3.77$. For phonon overlaps smaller than S_t^X—i.e., for $V_1'' > 3.77$—the ground state is totally symmetric, as shown in Fig. 5.

The temporal evolution of a system initially localized in one of the wells may now be determined by deriving expressions for the well states in terms of the SAS's. Clearly, we need to consider the possibility that the system has migrated to one of two distinct types of well. If we start off in well a, then, as can be seen in Fig. 4, we need to find the probability that the system has evolved to either one of the equivalent sets of nearest-neighbor wells $\{e,g,j\}$ or to one of the next-nearest-neighbor wells $\{b,c,d,f,h,i\}$. The (unnormalized) expressions for well states $|a\rangle$, $|b\rangle$, and $|e\rangle$ are found to be

$$|a\rangle = \frac{|A_a^{(t)}\rangle}{\sqrt{10}N_A^{(t)}} - \frac{|H_4^{(t)}\rangle + |H_5^{(t)}\rangle + |H_6^{(t)}\rangle}{\sqrt{6}N_H^{(t)}} - \frac{3|G_a^{(t)}\rangle - \sqrt{5}(|G_x^{(t)}\rangle + |G_y^{(t)}\rangle + |G_z^{(t)}\rangle)}{2\sqrt{15}N_G^{(t)}},$$

$$|b\rangle = \frac{|A_a^{(t)}\rangle}{\sqrt{10}N_A^{(t)}} - \frac{|H_4^{(t)}\rangle - |H_5^{(t)}\rangle - |H_6^{(t)}\rangle}{\sqrt{6}N_H^{(t)}} - \frac{3|G_a^{(t)}\rangle - \sqrt{5}(|G_x^{(t)}\rangle - |G_y^{(t)}\rangle - |G_z^{(t)}\rangle)}{2\sqrt{15}N_G^{(t)}},$$

$$|e\rangle = \frac{|A_a^{(t)}\rangle}{\sqrt{10}N_A^{(t)}} - \frac{\sqrt{2}|H_\theta^{(t)}\rangle - \sqrt{6}|H_\varepsilon^{(t)}\rangle + 2|H_4^{(t)}\rangle}{2\sqrt{6}N_H^{(t)}} + \frac{|G_a^{(t)}\rangle - \sqrt{5}|G_x^{(t)}\rangle}{\sqrt{15}N_G^{(t)}}, \tag{14}$$

where $|A_a^{(t)}\rangle$, $|G_j^{(t)}\rangle$ $(j=a,x,y,z)$, and $|H_j^{(t)}\rangle$ $(j=\theta,\epsilon,4,5,6)$ are the components of the SAS's of A, G, and H symmetry, respectively, involving the trigonal well states. The SAS normalization constants are given by

$$N_A^{(t)} = (1+S_t-2S_t^2)^{-1/2},$$

$$N_H^{(t)} = \sqrt{3}(3+S_t+2S_t^2)^{-1/2},$$

$$N_G^{(t)} = \sqrt{3}(3-S_t-2S_t^2)^{-1/2}. \tag{15}$$

Each of the states in Eq. (14) may be normalized by multiplication by the normalization constant

$$N^{(t)} = \sqrt{15}(15+2S_t-2S_t^2)^{-1/2}. \tag{16}$$

Using Eq. (14) and assuming that we are initially localized in the (normalized) well a, Eq. (3) implies that the probabilities of finding the system in well a, b, or e at time t are, respectively,

$$P_{aa}(t) = 1 - 15F_1\sin^2\left(\frac{\Delta_1 t}{2\hbar}\right) - 20F_2\sin^2\left(\frac{\Delta_2 t}{2\hbar}\right) - 12F_3\sin^2\left(\frac{\Delta_3 t}{2\hbar}\right),$$

$$P_{ab}(t) = \frac{1}{9}F_4 + 5F_1\sin^2\left(\frac{\Delta_1 t}{2\hbar}\right) + \frac{10}{9}F_2\sin^2\left(\frac{\Delta_2 t}{2\hbar}\right) - 2F_3\sin^2\left(\frac{\Delta_3 t}{2\hbar}\right),$$

$$P_{ae}(t) = \tfrac{1}{9}[3+2F_4+F_5-3P_{aa}(t)] - 2P_{ab}(t), \tag{17}$$

where the F_n are functions of S_t given by $F_n = F_n'/(15+2S_t-2S_t^2)^2$ with

$$F_1' = (1-S_t)(1+2S_t)(3+S_t+2S_t^2),$$

$$F_2' = (1-S_t)(3+2S_t)(3+S_t+2S_t^2),$$

$$F_3' = (1-S_t)^2(1+2S_t)(3+2S_t),$$

$$F_4' = S_t^2(1-16S_t)^2,$$

$$F_5' = S_t^2(11+4S_t)^2. \tag{18}$$

The interwell dynamics is clearly more complicated in this case because the system can migrate to two different sets of equivalent wells. Figure 6 shows examples of the temporal evolutions of the probabilities for three particular values of the phonon overlap. In Fig. 6(a), $S_t = 2S_t^X$ ($V_1'' \approx 3.09$) and the system is more weakly coupled than at the H-A crossover. Pseudorotation here is clearly fairly rapid with five reoccurrences of the initial localization occurring within the time period shown. In between the reoccurrences, the probability of finding the system in well a becomes quite small and the system is delocalized over the other wells. The situation is complicated with regard to the pseudorotational period but it does seem sensible to continue to use the defini-

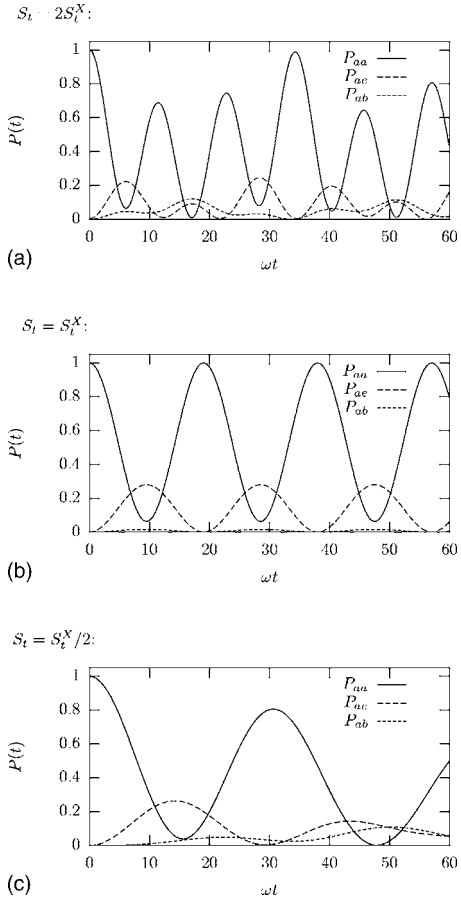

FIG. 6. Interwell dynamics for a trigonal system initially localized in well a. The variations for three different values of the phonon overlap are illustrated, where S_t^X is the phonon overlap between adjacent wells at the H-A crossover.

tion used in Sec. III A; that is, we define the pseudorotational period between trigonal wells $\mathcal{T}_t$ to be the time at which the first reoccurrence occurs. In Fig. 6(a), this occurs when $\omega\mathcal{T}_t \approx 11.5$. Prior to the first reoccurrence, the system becomes predominately localized in the nearest-neighbor wells $\{e,g,j\}$ and then, afterwards, in the next-nearest-neighbor wells $\{b,c,d,f,h,i\}$. Thus, we may also consider (albeit somewhat imprecisely) an average time taken for the system to migrate to nearest-neighbor and next-nearest-neighbor wells.

For coupling corresponding to the crossover point, $V_1'' \approx 3.77$, the situation is as shown in Fig. 6(b). Clearly, the dynamics is much more regular now and perfect reoccurrences of the initial state are observed. Pseudorotation is slower than before, and only three reoccurrences occur in the period shown. The pseudorotational period in this instance will be given exactly by the expression $\omega\mathcal{T}_t^X = 2\pi\hbar\omega/\Delta_2(S_t^X) \approx 19.05$. It is clear from this figure that, for this unique value of the linear coupling constant, the times taken for the system to pseudorotate to wells $\{e,g,j\}$ and $\{b,c,d,f,h,i\}$ are identical and are given by $\mathcal{T}_t^X/2$ (although the probabilities of rotating to those wells are different).

Finally, Fig. 6(c) shows the dynamics for the case when $S_t = S_t^X/2$ and the vibronic coupling constant $V_1'' \approx 4.35$ exceeds that at the crossover. The rate of pseudorotation has again decreased, and only one reoccurrence is visible in the plot. At the minima in P_{aa}, the system is delocalized over the other wells to degrees that vary with the minimum considered.

Suppose we now choose S_t $(0 < S_t \leq 1)$ to be rational, so that we can write

$$S_t = n/m, \tag{19}$$

where n and m are non-negative integers such that $m \neq 0$. Then, from Eq. (11), the ratio of the tunneling splitting is also rational and can be written as

$$\frac{\Delta_1}{\Delta_2} = \frac{N}{M}, \tag{20}$$

where integers N and M are given by the expressions

$$N = -2(3m+n)(m^2 - 8mn - 2n^2),$$

$$M = 3(m+2n)(3m^2 + 6mn - n^2). \tag{21}$$

Henceforth, we assume that N and M are given in their lowest terms and that $-2/3 < N/M < 1$, which follows from Eqs. (20) and (11). Next we define a characteristic time interval

$$\tau = \frac{2\pi\hbar N}{\Delta_1} \equiv \frac{2\pi\hbar M}{\Delta_2}. \tag{22}$$

It is clear from Eq. (17) that at this time $P_{aa}(\tau) \equiv 1$, $P_{ab}(\tau) \equiv F_4/9$, and $P_{ae}(\tau) \equiv F_5/9$; i.e., there has been a complete revival of the original state. For this reason, we shall refer to τ as the *master* pseudorotational period. In terms of the master period, Eq. (17) may be written as

$$P_{aa}(t) = 1 - 15F_1\sin^2\left(\frac{N\pi t}{\tau}\right) - 20F_2\sin^2\left(\frac{M\pi t}{\tau}\right) - 12F_3\sin^2\left[\frac{(N-M)\pi t}{\tau}\right], \tag{23}$$

so that further complete revivals will occur at times $t = 2\tau, 3\tau, \ldots$. However, partial revivals will also occur at earlier times. We can illustrate this by plotting Eq. (23) for various values of N and M.

Figure 7 shows the behavior when N is fixed at 1 and M is increased. The figure illustrates that the number of minima in $P_{aa}(t)$ in the interval $(0,\tau)$ is equal to M and that the approximate time for the first revival is τ/M. In the limit as $M \to \infty$, $\Delta_1 \to 0^+$ and $S \to S_t^X$, and we approach the H-A crossover. In this limit, Eq. (22) indicates that the master period $\tau \to \infty$ but the ratio $\tau/M = 2\pi\hbar/\Delta_2 \to 2\pi\hbar/\Delta_2(S_t^X)$. Thus, an approximate formula for the pseudorotation time (i.e., the time at which the first revival occurs) is

$$\mathcal{T}_t \approx \frac{2\pi\hbar}{\Delta_2}, \tag{24}$$

which will be exact at the crossover.

The effect of varying N is shown in Fig. 8. In creating this plot, we have intentionally taken M to be large and prime to help show the variation between plots. We see that the effect

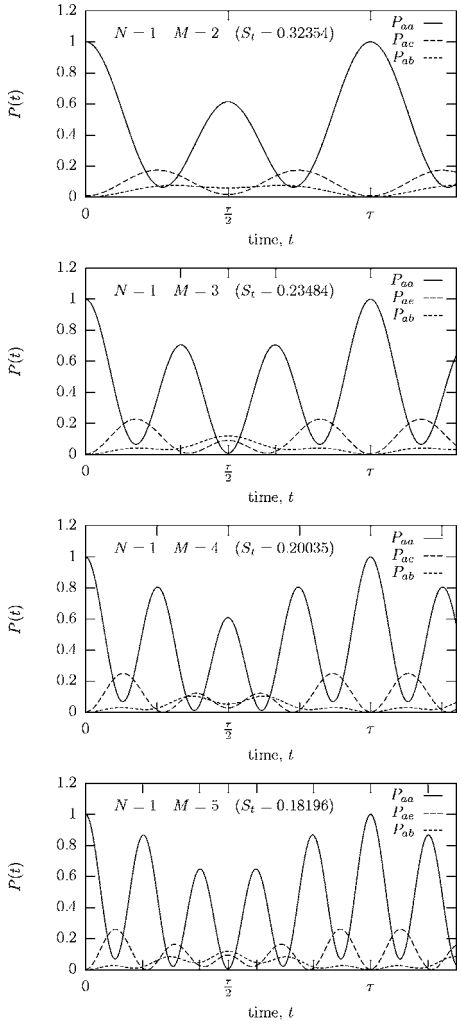

FIG. 7. Plots of the pseudorotation dynamics for a fixed value $N=1$ with increasing M. In the limit as $M\to\infty$, $S\to S_t^X$ and we approach the *H-A* crossover. In this limit, the partial revivals prior to $t=\tau$ become complete revivals.

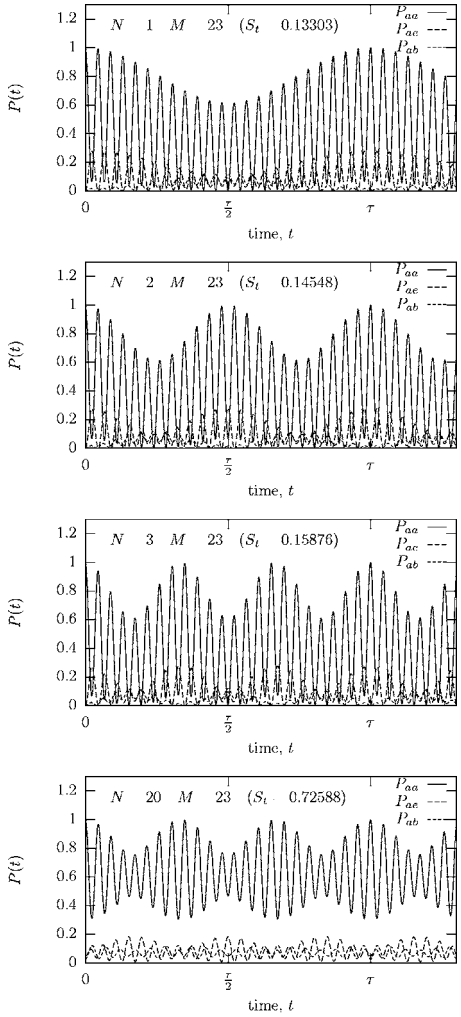

FIG. 8. Plots of the pseudorotation dynamics for a fixed value $M=23$ with increasing N. The probabilities are seen to be modulated by periodic functions with a period equal to $\max\{\tau/N, \tau/(M-N)\}$.

of N is to add a modulation to the probabilities, the frequency of the modulation increasing as N is increased from unity. However, the modulation when $N=k$ has the same period (but not form) as when $N=M-k$ and so the modulation frequency reaches a maximum when $N\sim M/2$. Thus, the modulation frequency is given by $\max\{\tau/N, \tau/(M-N)\}$.

An interesting corollary of the variations shown in Figs. 7 and 8 is that observation of the pseudorotational dynamics could give an indication of the vibronic coupling strength by simple consideration of the pattern of revivals. As an example, suppose we had observed experimentally the pseudorotational pattern associated with P_{aa} shown in Fig. 6(a), which appears to have two fairly equal partial revivals before reaching a complete revival. Following the foregoing discussion this would imply a situation akin to $N=1$ and $M=3$. This situation is consistent with a phonon overlap $S_t \approx 0.235$ which is fairly close to the value of $2S_t^X \approx 0.243$ used to draw the figure.

An approximate expression for the pseudorotation period has already been given in Eq. (24). An improved approximation may be found by looking for a formula for the period of the form

$$\mathcal{T}_t = \frac{2\pi\hbar}{\Delta_2} + \delta. \tag{25}$$

It is possible to derive an expression for δ by requiring that the time $\mathcal{T}_t$ defined in Eq. (25) be a solution to $\partial P_{aa}/\partial t=0$; i.e., $t=\mathcal{T}_t$ is a stationary point of $P_{aa}(t)$. This means that

$$15F_1 Q \sin\left(\frac{Q\Delta_2\mathcal{T}_t}{\hbar}\right) + 20F_2 \sin\left(\frac{\Delta_2\mathcal{T}_t}{\hbar}\right) + 12F_3(Q - 1)\sin\left[\frac{(Q-1)\Delta_2\mathcal{T}_t}{\hbar}\right] = 0,$$

where $Q=N/M$. We suppose that δ is small, such that $\delta \ll \min\{\hbar/|\Delta_1|, \hbar/|\Delta_2|, \hbar/|\Delta_1-\Delta_2|\}$. This allows us to expand each term in this expression in terms of δ—for example,

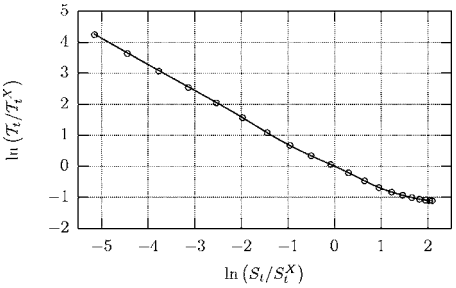

FIG. 9. Logarithmic plot of the approximate pseudorotational periods calculated using Eqs. (25) and (27) (solid line) compared to those calculated from P_{aa} numerically (∘). S_t^X and $\mathcal{T}_t^X$ are, respectively, the phonon overlap and pseudorotational period at the crossover.

$$\sin\left(\frac{Q\Delta_2\mathcal{T}_t}{\hbar}\right) = \sin(2\pi Q) + \cos(2\pi Q)\frac{Q\Delta_2\delta}{\hbar} + O(\delta^2). \tag{26}$$

Ignoring quadratic and higher terms in δ, this gives

$$\delta = \frac{3\hbar\ \tan(2\pi Q)[4F_3(1-Q) - 5F_1Q]}{\Delta_2[15F_1Q^2 + 20F_2\sec(2\pi Q) + 12F_3(1-Q)^2]}. \tag{27}$$

The pseudorotational periods calculated from this expression may be compared to those obtained numerically, as shown in Fig. 9, where the approximation is seen to be excellent over the range $0 \le V_1'' \le 7$ (chosen to coincide with the domain used in Fig. 5). The error induced by using Eqs. (25) and (27) to calculate the pseudorotational period increases with the vibronic coupling strength and amounts to ~2% when $V_1''=7$. We note that for the range of coupling constants considered, which should be great enough to encompass the values to be expected in C_{60}^+, the pseudorotational period varies by approximately two orders of magnitude. Hence, the results are shown using logarithmic scales for clarity.

IV. APPLICATION TO C_{60}^+ IONS

The results obtained so far pertain to a treatment of C_{60}^+ in terms of coupling between the H_u electronic state and a single vibrational mode of h_g symmetry. In a real C_{60}^+ ion, however, simultaneous coupling with eight h_g and six g_g modes needs to be included. Calculations of the vibronic coupling constants using density functional theory (DFT) indicate that the h_g modes are much more strongly coupled than the g_g modes and that the $h_g(1)$ mode (~261 cm^{-1}) makes, by far, the largest contribution.[5,9] The accuracy of these calculated coupling constants has been verified by using them to predict the $C_{60} \rightarrow C_{60}^+ + e^-$ photoemission spectrum, where excellent agreement with experiment was obtained.[21]

If we accept the dominance of the $h_g(1)$ mode and make use of the coupling constants computed using DFT,[5] then we can use the results given here to estimate the rate at which pseudorotation will occur between wells. The calculated coupling constants[5] indicate that $\mathcal{H}_1 \approx 0$ for mode $h_g(1)$, and so we expect the C_{60}^+ ion to be distorted into wells of D_{5d} symmetry. Furthermore, in terms of our dimensionless parameter we have $V_1'=1.52$. Using Eq. (6), this corresponds to a phonon overlap of $S_p=0.330$, and so using Eqs. (5) and (10), together with $\hbar\omega=261$ cm^{-1}, we arrive at $\mathcal{T}_p=210$ fs. Thus, we can expect that in order to detect pseudorotation between the D_{5d} wells in C_{60}^+, experiments must be performed on a femtosecond time scale. In addition, the interwell dynamics is expected to be quite simple and follow the trends shown in Fig. 3.

The predicted pseudorotational period of 210 fs may be viewed as a first approximation to the behavior of a true C_{60}^+ ion. A better value would be obtained by including all of the vibrational modes ($8h_g$ and $6g_g$) that couple to the electronic state. In such a multimode treatment, the Hamiltonian in Eq. (1) must be rewritten to include all 14 modes. As shown in an earlier work,[19] the ground APES arising from this multimode JT Hamiltonian can be successfully probed using a multidimensional minimization procedure. In this case, this involves a 64-dimensional optimization procedure. Nevertheless, the final outcome of such a procedure[19] is the realization of a set of potential minima.

Operation on any particular starting well by one of the group operators of the icosahedral group will, of course, yield just another of the wells. Thus, the number of wells is characteristic of the intrinsic symmetry of the wells as in the single-mode case; i.e., there may be six wells of D_{5d} or ten wells of D_{3d} symmetry. In the current example, as the $h_g(1)$ mode is calculated to dominate the distortion, we expect to find six D_{5d} wells with multimode characteristics. Once again, these six wells may be combined, using projection operators, to form SAS's possessing H and A symmetry. These SAS's will now have energies that depend on *all* of the energies of the coupled modes but are weighted in importance according to their coupling strengths.

Overall, we can envisage that the multimode picture will be very similar to the single-mode analysis given in Sec. III A. Thus, we expect to find pseudorotational behavior as depicted in Fig. 3. However, it will no longer be possible to simply relate the pseudorotational period, which is directly dependent on the tunneling splitting Δ, to one individual mode. This implies that experimental observation of pseudorotation in C_{60}^+ would give an overall measure of the strength of the vibronic coupling but would not, in itself, permit the coupling to individual modes to be discerned. However, observation of the pseudorotational dynamics should be a good indicator of the presence of D_{5d} rather than D_{3d} wells or vice versa.

V. DISCUSSION

To the best of our knowledge, no experiments have been performed to date that quantify pseudorotation in any JT system derived from C_{60}. However, it is clear from the work presented here that such experiments would give valuable information about the strength of the vibronic interactions in these systems. In an earlier paper, we outlined the principles underlying experiments that may be able to measure pseudorotation rates in certain derivatives of C_{60}.[17] This work is

still in progress. We note, however, that ultrafast optical experiments have already been used to observe pseudorotation in some simple $E \otimes e$ systems.[12] Therefore, it must only be a matter of time before determination of pseudorotation rates in more complicated systems, such as the ions derived from C_{60}, is possible.

In the current work, we have used a very simple method to derive analytical expressions for the pseudorotation characteristics of a somewhat idealized C_{60}^+ ion. The model used involves an "effective" or single-mode of vibration interacting with the electronic state. Fortuitously, this approach may not be too bad an approximation for C_{60}^+ because DFT calculations[5,9] seem to imply that the $h_g(1)$ mode is particularly strongly coupled in this ion. Using the calculated coupling constants for $h_g(1)$ alone, we estimate that pseudorotation in C_{60}^+ should occur with a period of ~210 fs. This gives some indication of the time scale of the pseudorotation and may be useful if experimental measurement is attempted.

If the $h_g(1)$ mode does dominate the vibronic interaction, then the C_{60}^+ ion is expected to be distorted into one of six isoenergetic molecular structures, each possessing D_{5d} symmetry, but differing in their orientation in a laboratory-fixed frame. Interconversion between these structures is expected to be "simple" (as in Fig. 3) because the five structures into which any particular starting structure can change are all equivalent. However, in the presence of other external perturbations, which do not favor the presence of D_{5d} configurations, it is plausible that the ion could be coerced into adopting D_{3d} structures. In this case, pseudorotation between the ten equivalent arrangements of the distorted ion will be more complex (as in Fig. 6). This complexity arises simply because of the fact that starting from any one particular D_{3d} well there are two different classes of other wells into which the system can pseudorotate. Therefore, such complex pseudorotational dynamics can be viewed as an indicator of the presence of D_{3d} distortion. However, a final complication that arises in the presence of D_{3d} minima means that the converse may not be necessarily true. That is, it is possible to have distortion into structures of D_{3d} symmetry but still observe simple pseudorotational dynamics [Fig. 6(b)]. This situation occurs at the *H-A* crossover and arises due to the fact that for this unique degree of vibronic coupling the time taken to pseudorotate from one particular well into any of the other wells becomes identical.

Another point worth reiterating here is that for other systems that are subject to different JT effects but that still may be coerced into D_{3d} minima—for example,[17] C_{60}^-—mere observation of the pseudorotational dynamics may give valuable information about the strength of the underlying vibronic coupling. This is because for these systems the dynamics is expected to consist of a series of "partial" and "complete" revivals which are characteristic of the degree of coupling. Interpretation of this pattern would be simple and lead to immediate conclusions concerning the vibronic interactions responsible. The dynamics of C_{60}^+ is somewhat more complicated.

ACKNOWLEDGMENT

We thank EPSRC (UK) for providing funds for this project.

*Electronic address: janette.dunn@nottingham.ac.uk; http://www.nottingham.ac.uk/~ppzjld

[1] A. F. Hebard, M. J. Rosseinsky, R. C. Haddon, D. W. Murphy, S. H. Glarum, T. T. M. Palstra, A. P. Ramirez, and A. R. Kortan, Nature (London) **350**, 600 (1991).
[2] M. J. Rosseinsky, A. P. Ramirez, S. H. Glarum, D. W. Murphy, R. C. Haddon, A. F. Hebard, T. T. M. Palstra, A. R. Kortan, S. M. Zahurak, and A. V. Makhija, Phys. Rev. Lett. **66**, 2830 (1991).
[3] S. Margadonna and K. Prassides, J. Solid State Chem. **168**, 639 (2002).
[4] O. Gunnarsson, J. E. Han, E. Koch, and V. H. Crespi, in *Superconductivity in Complex Systems*, edited by K. A. Müller and A. Bussmann-Holder, Vol. 114 of *Structure and Bonding* (Springer, Berlin, 2005), pp. 71–101.
[5] N. Manini, A. Dal Corso, M. Fabrizio, and E. Tosatti, Philos. Mag. B **81**, 793 (2001).
[6] O. Gunnarsson, Rev. Mod. Phys. **69**, 575 (1997).
[7] R. C. Haddon, L. E. Brus, and K. Raghavachari, Chem. Phys. Lett. **125**, 459 (1986).
[8] A. Ceulemans and P. W. Fowler, J. Chem. Phys. **93**, 1221 (1990).
[9] M. Saito, Phys. Rev. B **65**, 220508(R) (2002).
[10] S. E. Canton, A. J. Yencha, E. Kukk, J. D. Bozek, M. C. A. Lopes, G. Snell, and N. Berrah, Phys. Rev. Lett. **89**, 045502 (2002).
[11] N. Manini and E. Tosatti, Phys. Rev. Lett. **90**, 249601 (2003).
[12] J. Gaus, K. Kobe, V. Bonačić-Koutecký, H. Kühling, J. Manz, B. Reischl, S. Rutz, E. Schreiber, and L. Wöste, J. Phys. Chem. **97**, 12509 (1993).
[13] N. Manini, Phys. Rev. A **71**, 032503 (2005).
[14] C. P. Moate, M. C. M. O'Brien, J. L. Dunn, C. A. Bates, Y. M. Liu, and V. Z. Polinger, Phys. Rev. Lett. **77**, 4362 (1996).
[15] P. De Los Rios, N. Manini, and E. Tosatti, Phys. Rev. B **54**, 7157 (1996).
[16] I. D. Hands, J. L. Dunn, and C. A. Bates, Phys. Rev. B **73**, 014303 (2006).
[17] I. D. Hands, J. L. Dunn, and C. A. Bates, Phys. Rev. B **73**, 235425 (2006).
[18] M. Lüders, N. Manini, P. Gattari, and E. Tosatti, Eur. Phys. J. B **35**, 57 (2003).
[19] I. D. Hands, J. L. Dunn, W. A. Diery, and C. A. Bates, Phys. Rev. B **73**, 115435 (2006).
[20] C. P. Moate, J. L. Dunn, C. A. Bates, and Y. M. Liu, J. Phys.: Condens. Matter **9**, 6049 (1997).
[21] N. Manini, P. Gattari, and E. Tosatti, Phys. Rev. Lett. **91**, 196402 (2003).